Title	Fabrication of MoS2 nanowire arrays and layered structures via the self-assembly of block copolymers
Authors	Chaudhari, Atul;Ghoshal, Tandra;Shaw, Matthew T.;O'Connell, John;Kelly, Róisín A.;Glynn, Colm;O'Dwyer, Colm;Holmes, Justin D.;Morris, Michael A.
Publication date	2016-03-01
Original Citation	Chaudhari, A., Ghoshal, T., Shaw, M. T., O'Connell, J., Kelly, Roisin A., Glynn C., O'Dwyer C., Holmes, J. D. and Morris, M A. (2016) 'Fabrication of MoS2 Nanowire Arrays and Layered Structures via the Self#Assembly of Block Copolymers', Advanced Materials Interfaces, 3(11), 1500596 (9 pp). doi: 10.1002/admi.201500596
Type of publication	Article (peer-reviewed)
Link to publisher's version	http://onlinelibrary.wiley.com/doi/10.1002/admi.201500596/abstract - 10.1002/admi.201500596
Rights	© 2016 WILEY-VCH Verlag GmbH & Co. KGaA, Weinheim. This is the peer reviewed version of the following article: (2016). Fabrication of MoS2 Nanowire Arrays and Layered Structures via the Self#Assembly of Block Copolymers. Adv. Mater. Interfaces, 3: 1500596, which has been published in final form at https://doi.org/10.1002/admi.201500596. This article may be used for non-commercial purposes in accordance with Wiley Terms and Conditions for Self-Archiving.
Download date	2024-04-20 13:38:39
Item downloaded from	https://hdl.handle.net/10468/6308

Fabrication of MoS_2 Nanowire Arrays and Layered Structures *via* the Self-Assembly of Block Copolymers

Atul Chaudhari,[ab] Tandra Ghoshal,[ab] Matthew T. Shaw,[abc] John O'Connell,[a] Roisin A. Kelly,[a] Colm Glynn,[a] Colm O'Dwyer,[a] Justin D. Holmes[ab] and Michael A. Morris[*ab]

[a]Department of Chemistry and Tyndall National Institute, University College Cork, Cork, Ireland

[b]AMBER, Centre for Research on Adaptive Nanostructures and Nanodevices (CRANN), Trinity College Dublin, Dublin, Ireland.

[c]Intel Ireland Ltd., Collinstown Industrial Estate, Co. Kildare, Ireland

Email: m.morris@ucc.ie

Tel: +353 21 490 2180

Fax: +353 21 427 4097

The electronics industry is beginning to show interest in two dimensional molybdenum disulphide (2D-MoS_2) as a potential device material due to its low band gap and high mobility. However, current methods for its synthesis are not 'fab' friendly and require harsh environments and processes. Here, we report a novel method to prepare MoS_2 nanowire arrays and layered structures via self-assembly of a block copolymer system. Well-controlled films of microphase separated line-space nanopatterns have been achieved by solvent annealing process. The self-assembled films were used as 'templates' for the generation of non-stoichometric molybdenum oxide by in-situ inclusion technique following UV/Ozone treatment. Well-ordered array of MoS_2 and a layered structure was then prepared by chemical vapour deposition using sulphur powder at lower temperature. The surface morphology, crystal structure and phases were examined by different microscopic and spectroscopic techniques. This strategy could be extended to several other 2D materials system and open the pathway towards better optoelectronic and nanoelectromechanical systems.

Introduction

The transition-metal dichalcogenide semiconductor, molybdenum disulphide (MoS_2), a two-dimensional (2D) layered material, has attracted significant interest because of its distinctive electronic, optical, and catalytic properties, as well as its established use for dry lubrication.[1-17] An indirect-gap semiconductor, the bulk MoS_2 crystal, is built-up of van der Waals bonded S-Mo-S units and has a band gap of 1.29 eV and 1.90 eV for the bulk material and single layers, respectively.[18] MoS_2 field-effect transistors (FETs) have shown significant potential for fabrication of 2D electronic devices.[19-27] However, all the MoS_2 field-effect transistors (FETs) reported to date have been fabricated using electron beam or photo-lithography of MoS_2 flakes dispersed on substrates,[28-38] and/or polymer-assisted transfer of MoS_2 sheets followed by dissolving the effective adhesive used.[35] Both these processes involve multiple wet processing steps and the 2D structure formed are in direct contact with various wet chemicals which may contaminate or even degrade the MoS_2 surface. Different morphologies of MoS_2 can be synthesized by different methods such as

solvothermal, hydrothermal, high pressure-arc discharge and chemical transport reactions. Generally, the 2D materials are prepared by a two-step process: the synthesis of the layered bulk material which is followed by an exfoliation process.[39-41] Liu et al. performed a modified vacuum assisted impregnation route to synthesize highly ordered mesoporous MoS_2.[42] Ding et al. have obtained hierarchical MoS_2 microspheres via a facile PS microsphere-assisted hydrothermal method.[43] Surfactant assisted synthesis was also reported to improve the electrochemical performances. Liang et al. have reported the synthesis of MoS_2 nanosheets by an efficient and scalable PVP-assisted hydrothermal reaction.[44] There are a few well-known vapour phased synthesis methods involving the chemical reaction of sulphur and molybdenum compounds such as the thermal decomposition of ammonium thiomolybdate precursors in presence of hazardous gases like hydrogen sulphide (H_2S) and carbon disulphide (CS_2).[45-47]

The microphase separation of block copolymer (BCP) thin films can provide an alternative to conventional top-down lithographic methods. The BCP nanopatterns can be integrated into fabrication by removing one block of polymer and then using the remaining block of polymer as an etch mask for pattern transfer into the substrate.[48-50] As a variation of this methodology, different materials including various metal oxides, dielectric materials and metals have been combined with the BCP and used to create a hard mask to overcome the poor etch selectivity and shape control.[51-55]

In this paper, we systematically demonstrate the fabrication of monolayer and multilayer MoS_2 nanowire arrays by an alternative to conventional photolithographic processing, i.e. self-assembly of block copolymers followed by selective insertion of a Mo salt into the P4VP block and oxidation to form the metal trioxide. The MoS_2 nanowires were prepared with simple sulfurization of the molybdenum oxide (MoO_3). This method not only obviates the excessive use of wet chemistry steps, but also generates nanodimensioned wire-like patterns of 2D MoS_2 nanowires.

Experimental Section

Highly polished single-crystal silicon <100> wafers (p-type) with a native oxide layer of 2 nm were used. Two different molecular weight polystyrene-*block*-poly(4-vinylpyridine) (PS-*b*-P4VP) were purchased from Polymer Source, Inc., Canada, with a molecular weight of 37 kg mol-1 (Mn$_{PS}$ = 20 kg mol^{-1}, Mn$_{P4VP}$ = 17 kg mol^{-1}, f_{PS} = 0.54), with a polydispersity (Mw/Mn) of 1.08 and Mn = 18.2 kg mol^{-1} (Mn$_{PS}$ = 9 kg mol^{-1} , Mn$_{P4VP}$ = 9.2 kg mol^{-1}, f_{PS} = 0.49), with a polydispersity (Mw/Mn) of 1.09 (where, Mn and Mw are number average and weight average molecular weights). The block copolymer was used without further purification. Molybdenum (V) chloride ($MoCl_5$), toluene (99.8%, anhydrous), tetrahydrofuran (THF) (99.8%, anhydrous), ethanol (dehydrated, 200 proof) were purchased from Sigma-Aldrich and used without further purification.

In detail, the polymer was dissolved in a mixture of toluene and THF (80:20) to yield 0.5 wt% solution stirred for several hours to ensure complete dissolution prior to coating. BCP thin films were prepared by spin coating the polymer solution onto a substrate at 3000 rpm for 30 s. The thin films prepared were exposed to a saturated THF environment at 50ºC for 6 h. This solvent annealing procedure was carried out in 100 ml glass jar containing 10 ml of THF solvent in small vial. After six hours, samples were removed and trapped solvent allowed to evaporate under ambient conditions. Following this, a molybdenum (V) chloride solution of 0.5 wt% was prepared in ethanol and spin coated onto the phase separated film at 3000 rpm for 30s. UV/Ozone treatment was used to oxidize the precursor and remove the polymer. A UV/Ozone system (PSD Pro Series Digital UV Ozone system; Novascan Technologies, Inc., USA) was used to treat the sample in this way. This equipment has a UV source consisting of two low pressure mercury vapour grid lamps. Both lamps have an output current of 0.8-0.95 A and power of 65-100 W and have strong emissions at both wavelengths of UV radiation (184.9 nm and 253.7 nm). This system produces highly reactive ozone gas from oxygen that is present within the chamber. Samples were exposed for 3 h to ensure complete oxidization of the inorganic precursor and removal of the polymer. The thermal stability of the nanowires was verified by placing the substrate in the furnace at 700ºC for 1h.

Lee and co-workers have reported a method for synthesizing large-area MoS_2 monolayer flakes using the gas-phase reaction of MoO_3 and sulphur powders.[56] This was adapted here and MoO_3 wires prepared above were sulfurized using sulphur flowers at different temperatures and time (300, 400 and 700ºC for 30 , 20 and 15 min respectively). The thermal evaporation of sulphur was affected in a horizontal quartz tube furnace as shown in Figure 1. The samples were heated at heating rate of 15^{o}C min^{-1} under a H_2/Ar gas flow of 200 sccm. After sulfurization, the temperature ramped down at 15^{o}C min^{-1} until room temperature was reached.

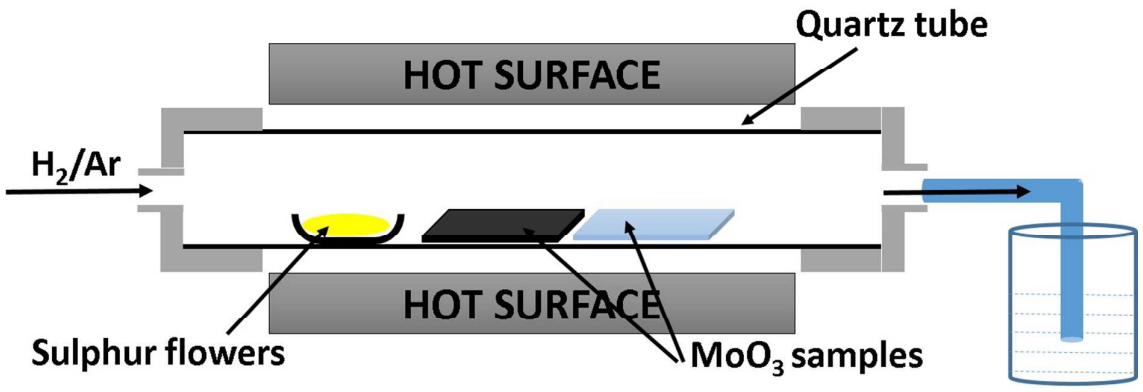

Fig.1 Experimental setup of the quartz tube in the centre of the furnace containing sulphur flowers and MoO_3 samples (see text for details).

BCP film thicknesses were measured by an optical ellipsometer (Woolam M2000). Surface morphologies were imaged by atomic force microscopy (SPM, Park systems, XE-100) in tapping mode using silicon microcantilever probe tips with a force constant of 60000 Nm^{-1} and a scanning force of 0.11nN. Both topographic and phase images were recorded simultaneously. Scanning electron microscopy (SEM, FEI Helios NanoLab 600 Dual Beam FIB and Raith eLINE Plus) was also used to study the surface morphology. X-Ray photoelectron spectroscopy (XPS) experiments were conducted on a Vacuum Science Workshop CLASS100 high performance hemispherical analyser using Al Kα radiation (hν = 1486.6 eV). Raman scattering spectroscopic data were collected with a Renishaw inVia Raman spectrometer using a 514 nm 30 mW Argon Ion laser and spectra were collected using a RenCam CCD camera. The beam was focused onto the samples

using either a 20x or a 50x objective lens. Spectra were collected at a variety of exposure times and laser intensities. TEM cross-sections (lamellae) were prepared using a Helios Nanolab DB focused ion beam (FIB). FIB samples were analysed by JEOL 2100 high resolution TEM operating at an accelerating voltage of 200 kV.

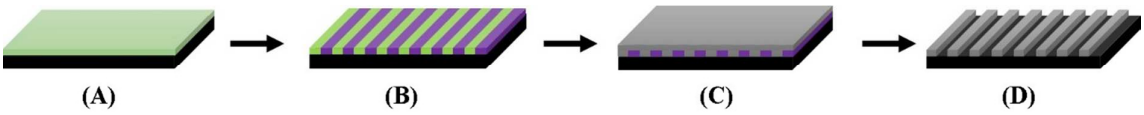

Scheme 1 Schematic of the formation of the MoO_x nanowires. (A) PS-*b*-P4VP BCP spin coated on silicon wafer, (B) phase separated BCP thin film after solvent annealing, (C) loading of molybdenum precursor on/in the P4VP domains by spin coating and (D) fabrication of MoO_x nanowires by UV/Ozone treatment.

Scheme 1 shows the overall methodology of producing molybdenum oxide nanowires. The strategy involves the formation of a well-defined microphase separated BCP nanopattern. Briefly, the BCP was spin coated onto a silicon wafer (A) and then microphase separated under solvent vapor annealing (SVA) (B). The molybdenum precursor solution was then spin coated onto the phase separated BCP film (C). Finally, UV/Ozone treatment was carried out for 3h which led to the formation of regular structure of MoO_x.

In the following, we develop a well-defined MoS_2 pattern using techniques described above. Work will be centred on the large size PS_{20k}-*b*-$P4VP_{17k}$ system since similar results were seen with both polymers used. Indicative results from the smaller block systems are detailed towards the end of the paper.

As-cast PS_{20k}-*b*-$P4VP_{17k}$ thin films are kinetically trapped in a micellar arrangement as can be clearly seen in Fig. 2A. Thin films solvent annealed in a THF environment for 6h at 50ºC generate vertically aligned lamellar nanostructures of pitch size (domain spacing) 37 nm, as shown in Fig. 2B. The morphology and orientation of the films is dependent on careful choice of annealing

solvent and conditions as discussed elsewhere.[57, 58] The thickness of the film was measured by elliposmetry and found out to be ~32 nm, close to the domain spacing.

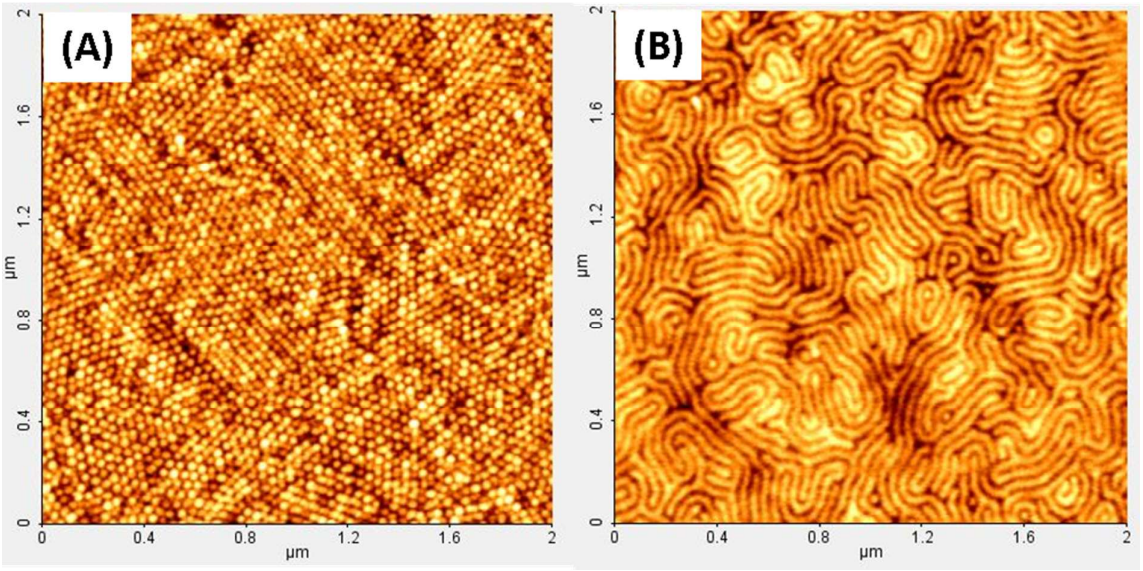

Fig. 2 AFM topographic images of (A) as-cast and (B) phase separated PS-*b*-P4VP thin films after solvent annealing in THF for 6 h at 50^{o}C

The BCP films can be used as 'templates' to create ordered oxide nanowire arrays by the salt inclusion technique described above.[59, 60] When ethanol was added to $MoCl_5$, an emerald green solution is obtained, due to the formation of the dimer $[MoCl_3(OR)_2]_2$.[61] To prevent overfill and non-selective salt deposition at the film surface of the BCP, a low concentration of precursor solution is required and a 0.5 wt.% $MoCl_5$ solution was found to be optimum for spin coating. Typical samples following UV/Ozone treatment for 3 h are shown in Fig. 3A (topographic AFM) and Figure 3B of the Mo oxide structures formed. The MoO_x structure formed by inclusion was similar to that of the original BCP with a pitch size of 37 nm. The SEM magnified view of the surface (Figure 3C) displays features with sharp edges and relatively smooth surfaces consistent with crystalline materials.

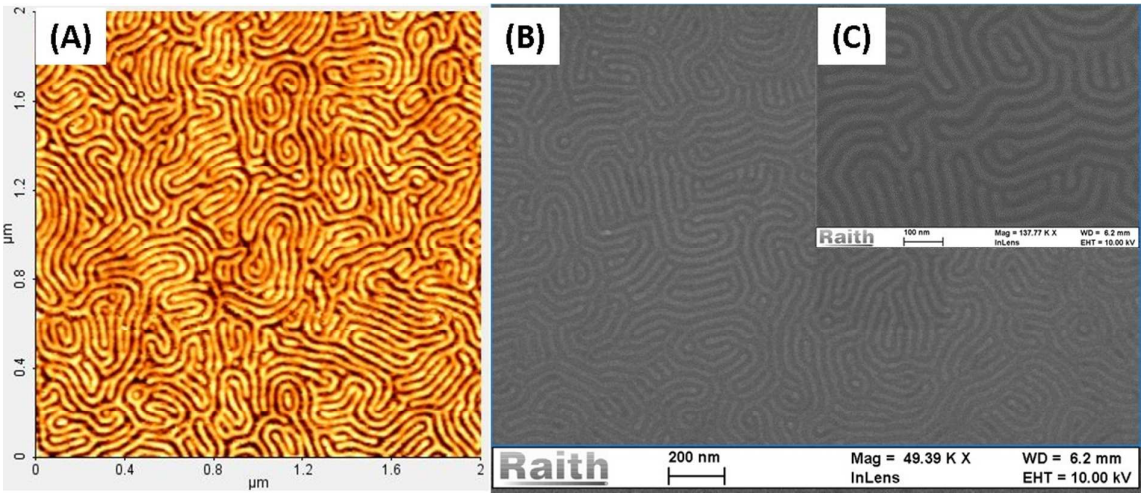

Fig. 3 AFM topography image (A), top-down SEM image (B) and (C) is SEM image of same sample at higher magnification of molybdenum oxide nanowires obtained after UV/Ozone treatment of self-assembled PS_{20k}-*b*-$P4VP_{17k}$ for 3h.

X-ray photoelectron spectroscopy (XPS) analysis of the Mo oxide nanowires prepared above was performed in order to determine the chemical composition of the samples. Since these are thin (see below) it is suggested this is indicative of the bulk composition of the wires. The XPS survey spectrum shows main features due to molybdenum and oxygen and minor peaks of carbon and silicon (Fig. 4A). The scan shows no evidence of surface charging effects and no features due to impurities such as Cl could be seen. The carbon feature (C1*s* at 285.1 eV) is consistent with adventitious contamination. The appearance of Si 2*s* and Si 2*p* signals are attributed to the Si substrate used. The Mo 3*d* features (Fig. 4B) are typical of Mo in the 6+ oxidation state [62-68] with Mo $3d_{5/2}$ and Mo $3d_{3/2}$ at binding energies (BE) of 232.3 eV and 235.5 eV.

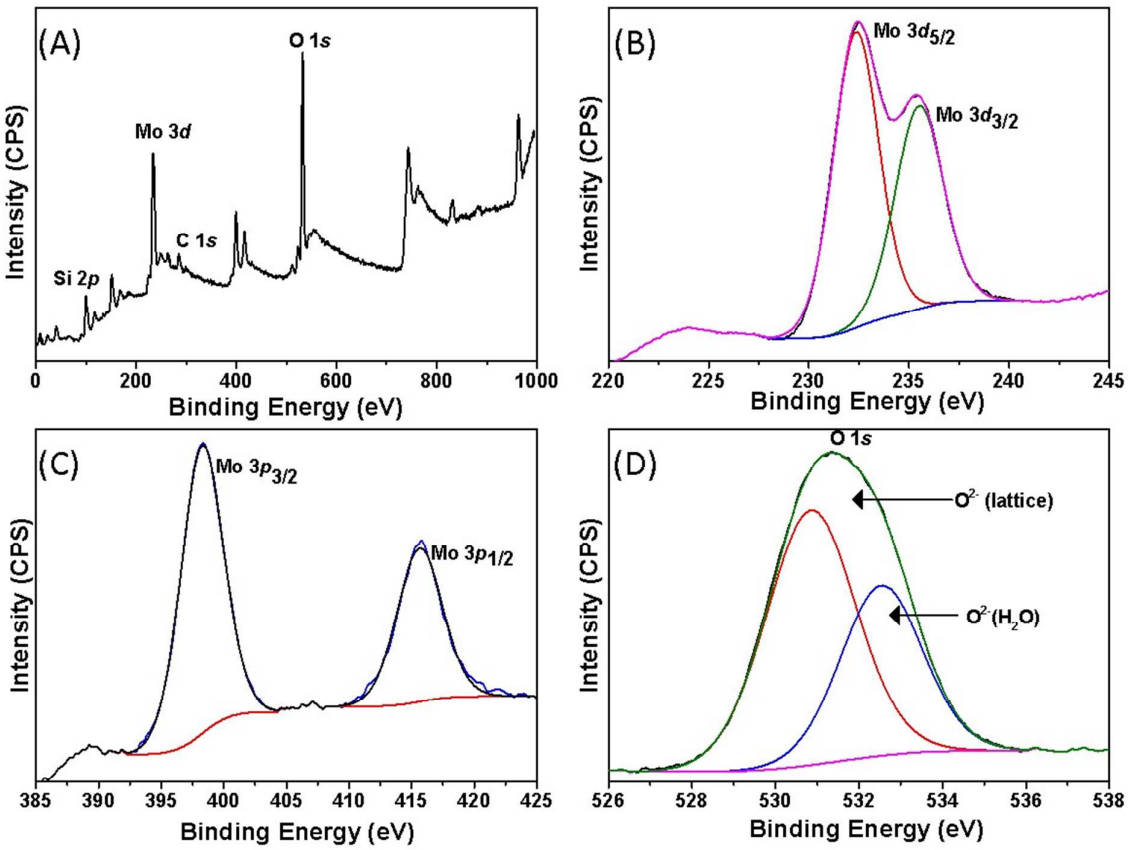

Fig. 4 XPS spectra of (A) wide scan spectra (survey), (B) Mo 3*d*, (C) Mo 3*p* and (D) O 1*s* core level spectra of molybdenum oxide nanowires after UV/Ozone treatment.

As shown in Fig. 4C, the two components associated with Mo $3p_{3/2}$ and Mo $3p_{1/2}$ spin orbit doublet at 398.2 eV and 415.6 eV BE respectively are also in agreement with the literature value.[69] Complete hydrolysis/oxidation of the Mo precursor solution was also confirmed as no chlorine can be detected on extensive XPS investigation. The O 1*s* peaks of the XPS spectra of the same films are shown in Fig. 4D. The asymmetric O1s feature can be resolved into two features (using standard curve-fitting procedures) at ~531 eV and 532.5 eV and these can be interpreted as lattice oxygen (O^{2-}) and surface hydroxyl/adsorbed water species respectively. Note that the O 1*s* signal at ~531 eV is quite broad possibly because of a contribution of a range of different lattice oxygen sites in the MoO_3 structure and also signal deriving from the passive oxide coated silicon substrate.

The fabricated MoO_3 nanowires on silicon substrates were subject to sulphur treatments for different temperature/times as described above. These conditions were varied to ensure that the

MoO_3 nanowires could be fully converted to the sulfide derivatives. Fig. 5 shows typical SEM data from selected samples but in each case the contrast changes (compared to the oxide only samples) are consistent with composition changes.

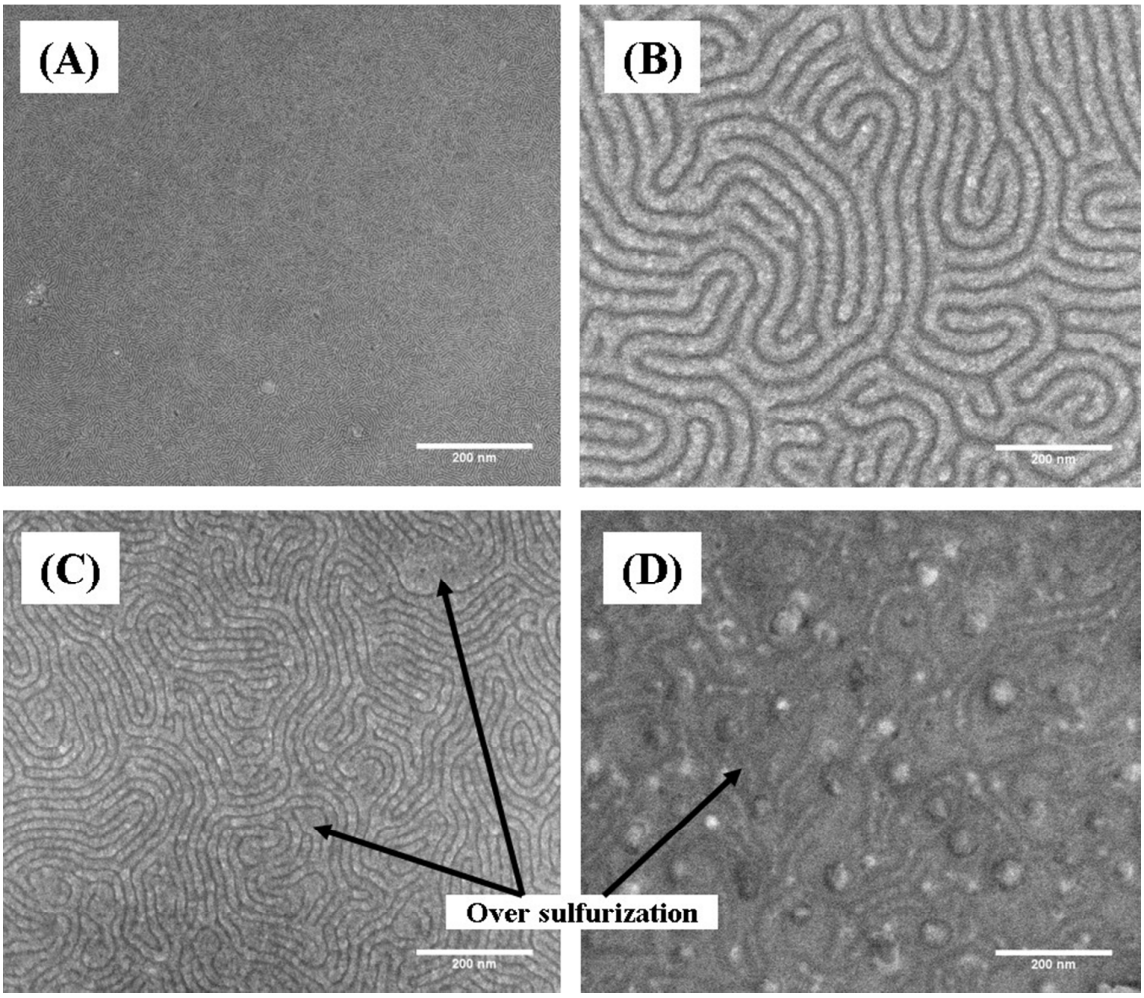

Fig. 5 Scanning electron micrographs of MoS_2 nanowires formed after sulfurization of MoO_3 nanowires by thermal evaporation of sulphur powders at: (A-B) 300^{o}C for 30 min, (C) 400^{o}C for 20 min and (D) 700ºC for 15 min.

At the lowest temperature of 300^{o}C the nanowires formed are not damaged or delaminated from the substrate and the structures remain intact (Fig. 5A). It is thought that in the conditions used the MoO_3 is readily reduced to MoO_2,[70] which is then converted to the sulphide. The higher magnification image (Fig. 5B) confirms the gross morphology of the nanopattern is not disturbed. Higher temperature processes appear to cause the degradation of the pattern with clear evidence of

over-sulfurization as shown in Fig. 5C-D. At 400°C (Fig. 5C) the SEM image appears to be similar to the image of the MoS_2 formed at 300ºC but the structure is not uniform and in several areas the wires coalesce. After reaction at 700ºC (Fig. 5D), obvious degradation has occurred. Much of the nanowire pattern is lost and evidence or the nucleation of particulate is observed. This suggests that a nucleation and growth mechanism for MoS_2 through surface diffusion exists at higher temperature.

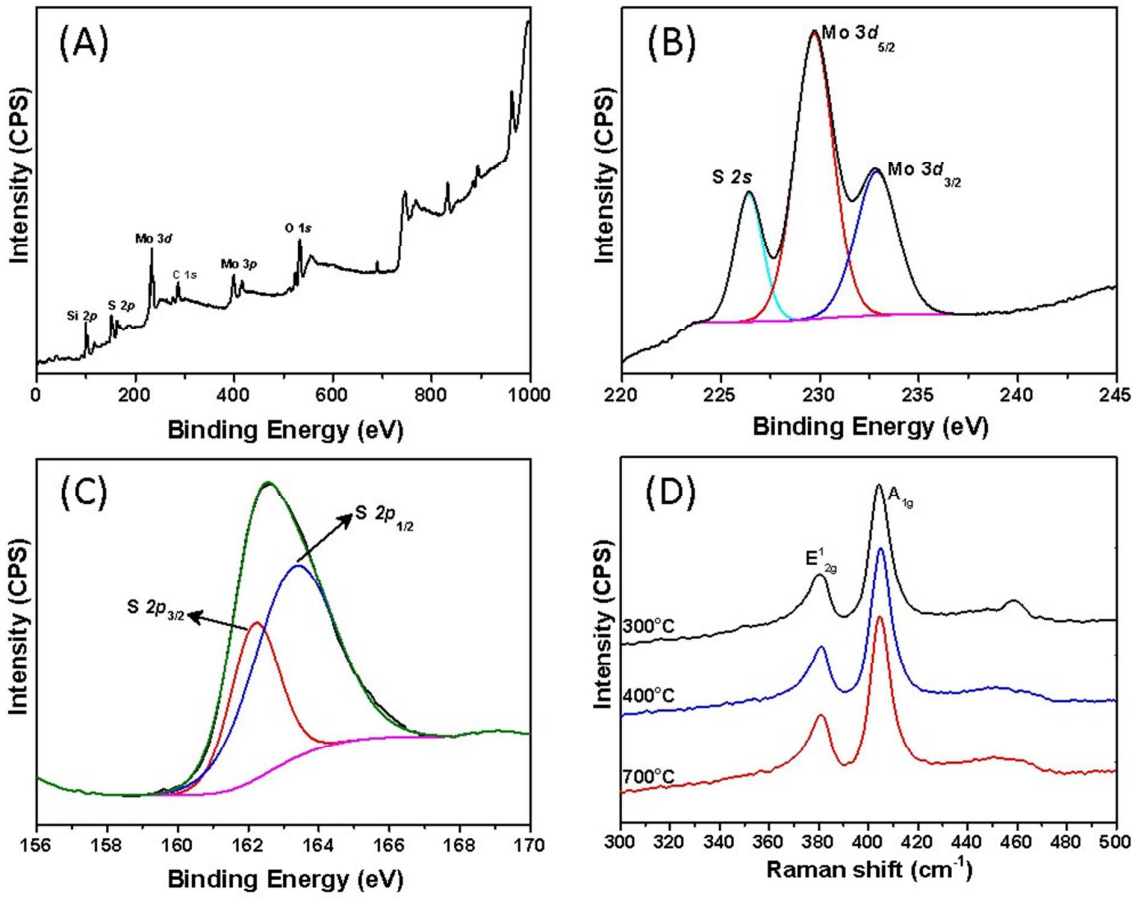

Fig. 6 MoS_2 nanopatterns analyzed by XPS and Raman spectroscopy. (A) XPS survey spectrum of the MoS_2 prepared at 300ºC. High resolution XPS spectra of (B) Mo 3*d* and S 2*s*; and (C) S 2*p*. (D) Raman spectrum of MoS_2 nanowires formed after sulfurization at 300, 400 and 700ºC showing the E^1_{2g} and A_{1g} vibrational modes

For all three samples, as shown in Fig. 6, XPS analysis was carried out to study the chemical composition and the surface electronic states of MoS_2. The XPS survey spectrum (Fig. 6A)

indicates the presence of Mo, S, C and O elements. In Fig. 6B-C, high-resolution XPS spectra of Mo 3*d* and S 2*p* are shown, respectively. The Mo 3*d* spectra displays peaks around 229.7 and 232.7 eV ($Mo3d_{5/2}$ and $Mo3d_{3/2}$ respectively) and these are similar to features typical of Mo^{4+} states in MoS_2.[71] The smaller peak visible (Fig. 6B) at 226.4 eV is identified as the S2*s* feature. The atomic ratio of Mo:S determined from the peak area ratio is 1:1.95 consitent with MoS_2. The S2*p* photoelectron spectrum is shown in Fig. 6C, and shows a broad single peak at 162.5 eV due to overlapping $S2p^{3/2}$ and $2p^{1/2}$ peaks of S^{2-} in MoS_2.[72, 73] Raman spectroscopy was carried out to analyse the structure and it further confirmed the MoS_2 structure with the appearance of two distinct peaks at 381 cm^{-1} and 405 cm^{-1}. These are consistent with the E^1_{2g} vibrational Mo-S bond along the base plane and the A_{1g} vibration of sulphur along the vertical axis, respectively.[74] At 300ºC, a small shoulder peak was observed at about 460 cm^{-1} due to the presence of MoO_2.[75] This suggests incomplete sulfurization at the lower temperatures used. With increasing temperature the Raman features remained narrow and is consistent with the presence of highly ordered layered structures. The peak difference between A_{1g} and E_{2g} modes (24 cm^{-1}) can be used to identify the number of layers of MoS_2 which gives 4-5 layers.[74, 76]

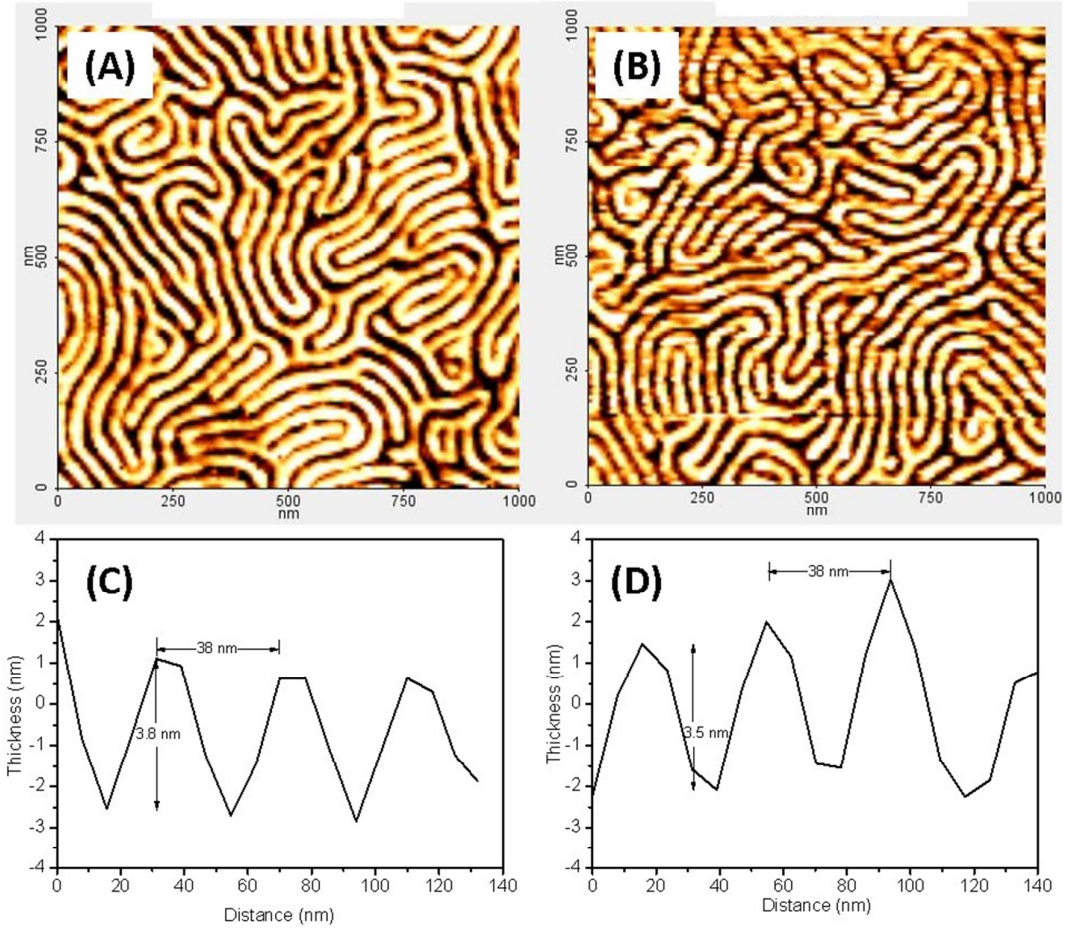

Fig. 7 (A) and (B) are the topographic AFM images of MoO_3 and MoS_2 nanowires, (C) and (D) are the height profiles of (A) and (B) respectively.

The value of the MoS_2 thickness calculated by the Raman method can be compared to that calculated by AFM. Fig. 7 shows the multilayer MoO_3 and MoS_2 nanowires and their height profiles by AFM. An analysis of the data in Figure 6 shows that the distance between the MoO_3 and MoS_2 nanowires (pitch) is 38 nm consistent with the original BCP structure. However the measured thicknesses for the oxide is 3.8 nm and 3.5 nm for the sulfide MoS_2. The monolayer thickness of S-Mo-S structures in bulk MoS_2 have a thickness of 0.6 nm.[77, 78] This suggest a shade of around 6 MoS_2 layers in reasonable agreement with the Raman measured value.

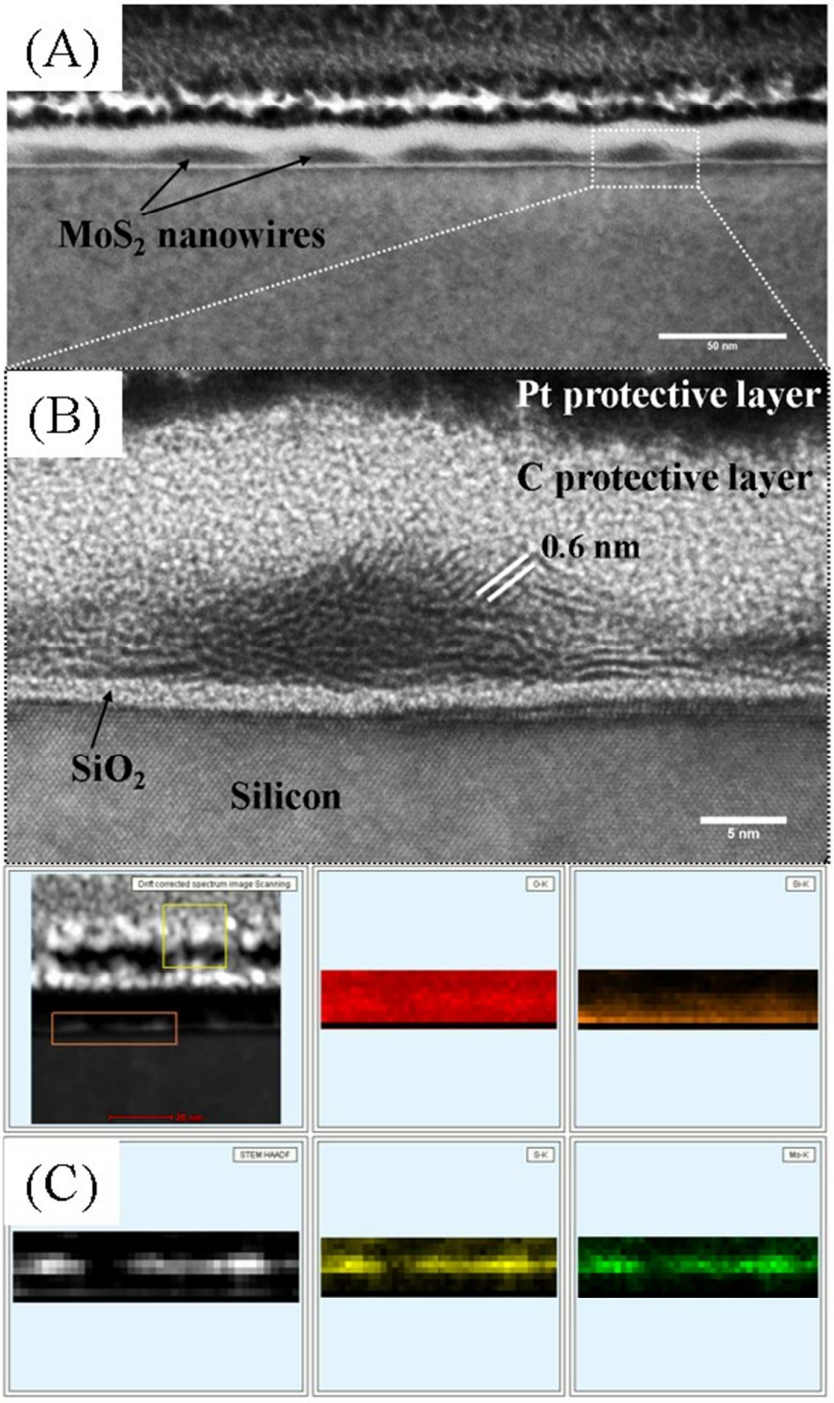

Fig. 8 (A) TEM images of MoS_2 nanowires. (B) Enlarged HR-TEM image of the marked area in (A). (C) EDX mapping of MoS_2 nanowire revealing presence of S and Mo.

The final morphology of the multilayer MoS_2 formed by sulfurization at 300^{o}C for 30 min was studied by TEM FIB cross section and a typical image is shown in Fig. 8. It can be seen immediately that the top-down nanowire pattern extends through to the substrate (Fig. 8A). The

nanowire structures seem to be somewhat different than might be expected from ideal rectangular cross-sections. The nanowires show a rounded shape and indications of spreading at the base or even the formation of a surface layer of MoS_2 during preparation (e.g. via a P4VP wetting layer). However, the latter seems less likely as in several areas distinct gaps are seen between the wire bases. The observation of broadening might be expected since the melting point of MoO_3 is relatively low at less than 800ºC[79] and we suggest the broadening of features results from diffusion processes. In Fig. 8B, the high resolution TEM cross-section data confirm that the MoS_2 nanowires have a well-defined layer structure although the structure is clearly polycrystalline in nature and not preferentially orientated with reference to the surface plane. There are clearly a few layers of MoS_2 on top of the SiO_2/Si substrates and the average height of these is 6 to 8 nm or 10-12 layers. This is somewhat higher than the value seen by AFM but this may be related to tip issues in small dimensioned topography as well as the averaging nature of Raman which will provide an average thickness across the substrate surface. As shown in Fig. 8C, the high angle annular dark-field scanning transmission electron microscopy (HAADF-STEM) image indicates the presence of MoS_2 nanowires on Si-substrate. To confirm the presence of MoS_2 nanowire after the sulfurization, energy dispersive X-ray (EDX) mapping was performed to reveal presence of S (yellow) and Mo (green).

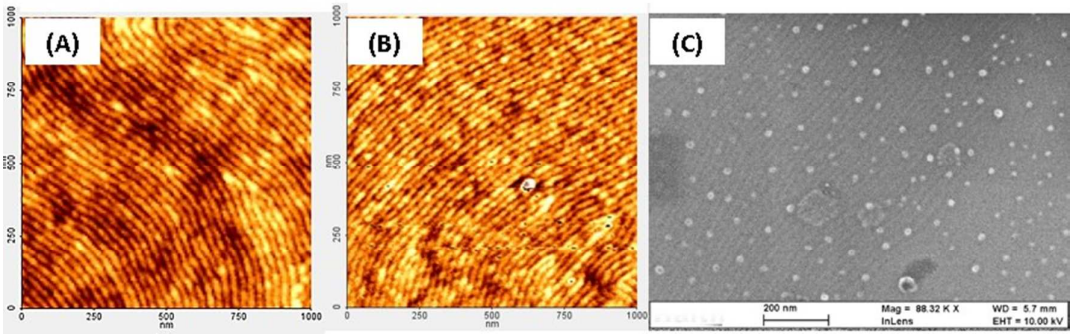

Fig. 9 (A) is the AFM topography images of PS_{9k}-b-$P4VP_{9.2k}$ after solvent annealing in THF for 6 h at 50ºC, (B) is the topographic AFM image of the MoO_3 nanowires obtained after UV/Ozone treatment of sample shown in (A), and (C) is SEM image of the MoS_2 nanowires obtained after sulfurization at 300ºC.

This form of BCP nanofabrication is extremely versatile and can be used to create nanopatterns of different dimensions by varying the molecular weight of the polymer. In order to verify that the methodology could be extended to lower molecular weight systems and, hence, smaller feature size, a further set of the experiments were performed using the lower molecular weight PS_{9k}-*b*-$P4VP_{9.2k}$ with total molecular weight of 18.2 kg mol^{-1}. Fig. 9A illustrates the lamellar structure formed after solvent annealing the PS_{9k}-*b*-$P4VP_{9.2k}$ at 50ºC for 6h in a THF atmosphere. The long range well-defined and ordered lamellar morphology of the BCP over several micrometres can be readily seen in the image and a domain (pitch) size of 23 nm was measured. Fig. 9B-C provides a view of the derived MoO_3 and MoS_2 (300ºC sulfurization) nanopatterns formed after similar experimental procedure to that described above. As for the higher molecular weight BCP, the oxide and sulfide nanowires have similar morphology to the templating microphase separated BCP structure and indicate the robust nature of the fabrication process used. Interestingly, nucleation of sulfide nanoparticles is seen at this lower temperature in contrast to the higher molecular weight structure where sulfurization did not produce aggregates until higher temperatures. This is consistent with a mass-transport limited growth or sintering process since these limitations are reduced for the smaller, more densely packed nanofeatures produced by lower molecular weight BCPs.

Conclusions

In summary, we have demonstrated the fabrication of MoS2 nanowires by using simple and cost effective BCP approach. The self-assembly of block copolymers has already received attention as an alternative method to the current UV-lithographic process for producing Si nanowires but the use of the methodology outlined here could be adapted to allow the direct formation of a range of nanowire materials. There are real challenges in developing methods for the fabrication of nanometre dimensioned patterns of 2D materials such as low-band gap MoS_2 where etching and selective chemistries can either alter the stoichiometry or easily prepared materials such as flakes are difficult to integrate into large scale production. In this article we propose a two-step process to synthesize large-area and polycrystalline MoS_2 nanowire thin layers. The self-assembly of PS-*b*-

P4VP block copolymers have been shown to be a convenient and readily processable method for the preparation of MoS_2 nanowires of thicknesses equivalent to a few layers of MoS_2. The structures obtained here are free of chlorine after oxidation by UV/Ozone treatment as confirmed by XPS despite the use of a chloride salt precursor. Large-area MoS_2 films were the directly synthesized on SiO_2/Si substrates by sulfurization of the patterned MoO_3 thin film formed by an insertion and oxidation process. The obtained structures were characterized and confirmed as MoS_2 layered systems by a range of techniques such as AFM, XPS, Raman, SEM and TEM.

The sulfurization strategy used here was performed at relatively low temperatures, however, elevated temperatures resulted in agglomeration and growth of 3D particles. Even at the lowest temperatures, the mass transport and diffusion led to broadening of the wire bases as evidenced by high resolution, cross-section TEM. This may be associated with the low melting point of MoO_3. Thus, in order to produce nanowires as electronic circuitry, careful optimization of the sulfurization route will be required. However, the techniques outlined here may provide a breakthrough in the fabrication of patterned structures of complex materials.

Acknowledgements

We thank Dr. Subhajit Biswas for assistance with sulfurization experiments. We acknowledge financial support from the Science Foundation Ireland (SFI) AMBER grant 12/RC/2278 and Semiconductor Research Corporation (SRC) grant 2013-OJ-2444. We also thank Anushka Gangnaik for help with microscopic analysis.

References:

1. In *Physics and chemistry of materials with layered structures*, ed. P. A. Lee, Springer Netherlands1976, vol. 4, pp. VIII, 464.
2. R. A. Bromley, R. B. Murray and A. D. Yoffe, *Journal of Physics C: Solid State Physics*, 1972, **5**, 759.
3. R. V. Kasowski, *Physical Review Letters*, 1973, **30**, 1175-1178.
4. L. F. Mattheiss, *Physical Review Letters*, 1973, **30**, 784-787.
5. L. F. Mattheiss, *Physical Review B*, 1973, **8**, 3719-3740.

6. R. Coehoorn, C. Haas and R. A. de Groot, *Physical Review B*, 1987, **35**, 6203-6206.

7. R. Coehoorn, C. Haas, J. Dijkstra, C. J. F. Flipse, R. A. de Groot and A. Wold, *Physical Review B*, 1987, **35**, 6195-6202.

8. A. R. Beal and H. P. Hughes, *Journal of Physics C: Solid State Physics*, 1979, **12**, 881.

9. A. R. Beal, J. C. Knights and W. Y. Liang, *Journal of Physics C: Solid State Physics*, 1972, **5**, 3540.

10. T. Böker, R. Severin, A. Müller, C. Janowitz, R. Manzke, D. Voß, P. Krüger, A. Mazur and J. Pollmann, *Physical Review B*, 2001, **64**, 235305.

11. B. L. Evans and P. A. Young, *Proceedings of the Royal Society of London A: Mathematical, Physical and Engineering Sciences*, 1965, **284**, 402-422.

12. B. L. Evans and P. A. Young, *Proceedings of the Physical Society*, 1967, **91**, 475.

13. K. K. Kam and B. A. Parkinson, *The Journal of Physical Chemistry*, 1982, **86**, 463-467.

14. T. Li and G. Galli, *The Journal of Physical Chemistry C*, 2007, **111**, 16192-16196.

15. J. C. McMenamin and W. E. Spicer, *Physical Review B*, 1977, **16**, 5474-5487.

16. J. A. Wilson and A. D. Yoffe, *Advances in Physics*, 1969, **18**, 193-335.

17. X. Zong, H. Yan, G. Wu, G. Ma, F. Wen, L. Wang and C. Li, *Journal of the American Chemical Society*, 2008, **130**, 7176-7177.

18. K. F. Mak, C. Lee, J. Hone, J. Shan and T. F. Heinz, *Physical Review Letters*, 2010, **105**, 136805.

19. B. W. H. Baugher, H. O. H. Churchill, Y. Yang and P. Jarillo-Herrero, *Nano Letters*, 2013, **13**, 4212-4216.

20. H. Fang, M. Tosun, G. Seol, T. C. Chang, K. Takei, J. Guo and A. Javey, *Nano Letters*, 2013, **13**, 1991-1995.

21. D. Fu, J. Zhou, S. Tongay, K. Liu, W. Fan, T.-J. King Liu and J. Wu, *Applied Physics Letters*, 2013, **103**, 183105.

22. H. Liu, M. Si, Y. Deng, A. T. Neal, Y. Du, S. Najmaei, P. M. Ajayan, J. Lou and P. D. Ye, *ACS Nano*, 2014, **8**, 1031-1038.

23. B. Radisavljevic and A. Kis, *Nat Mater*, 2013, **12**, 815-820.

24. B. Radisavljevic, M. B. Whitwick and A. Kis, *ACS Nano*, 2011, **5**, 9934-9938.

25. B. Radisavljevic, A. Radenovic, J. Brivio, V. Giacometti and A. Kis, *Nat Nano*, 2011, **6**, 147-150.

26. H. Wang, L. Yu, Y. Lee, W. Fang, A. Hsu, P. Herring, M. Chin, M. Dubey, L. Li, J. Kong and T. Palacios, *Electron Devices Meeting (IEDM), 2012 IEEE International*, 2012.

27. H. Wang, L. Yu, Y.-H. Lee, Y. Shi, A. Hsu, M. L. Chin, L.-J. Li, M. Dubey, J. Kong and T. Palacios, *Nano Letters*, 2012, **12**, 4674-4680.

28. W. Bao, X. Cai, D. Kim, K. Sridhara and M. S. Fuhrer, *Applied Physics Letters*, 2013, **102**, 042104.

29. H.-Y. Chang, S. Yang, J. Lee, L. Tao, W.-S. Hwang, D. Jena, N. Lu and D. Akinwande, *ACS Nano*, 2013, **7**, 5446-5452.

30. S. Das and J. Appenzeller, *physica status solidi (RRL) – Rapid Research Letters*, 2013, **7**, 268-273.

31. S. Das, H.-Y. Chen, A. V. Penumatcha and J. Appenzeller, *Nano Letters*, 2013, **13**, 100-105.

32. L. Jongho, C. Hsiao-Yu, H. Tae-Jun, L. Huifeng, R. S. Ruoff, A. Dodabalapur and D. Akinwande, *Electron Devices Meeting (IEDM), 2013 IEEE International*, 9-11 Dec. 2013; 2013; 19.2.1

33. S. Kim, A. Konar, W.-S. Hwang, J. H. Lee, J. Lee, J. Yang, C. Jung, H. Kim, J.-B. Yoo, J.-Y. Choi, Y. W. Jin, S. Y. Lee, D. Jena, W. Choi and K. Kim, *Nat Commun*, 2012, **3**, 1011.

34. D. J. Late, Y.-K. Huang, B. Liu, J. Acharya, S. N. Shirodkar, J. Luo, A. Yan, D. Charles, U. V. Waghmare, V. P. Dravid and C. N. R. Rao, *ACS Nano*, 2013, **7**, 4879-4891.

35. G.-H. Lee, Y.-J. Yu, X. Cui, N. Petrone, C.-H. Lee, M. S. Choi, D.-Y. Lee, C. Lee, W. J. Yoo, K. Watanabe, T. Taniguchi, C. Nuckolls, P. Kim and J. Hone, *ACS Nano*, 2013, **7**, 7931-7936.

36. H. Liu, A. T. Neal and P. D. Ye, *ACS Nano*, 2012, **6**, 8563-8569.

37. H. Liu and P. D. Ye, *Electron Device Letters, IEEE*, 2012, **33**, 546-548.

38. H. Nam, S. Wi, H. Rokni, M. Chen, G. Priessnitz, W. Lu and X. Liang, *ACS Nano*, 2013, **7**, 5870-5881.

39. M. Chhowalla and G. A. J. Amaratunga, *Nature*, 2000, **407**, 164-167.

40. D. Duphil, S. Bastide and C. Levy-Clement, *Journal of Materials Chemistry*, 2002, **12**, 2430-2432.

41. M. Virsek, M. Krause, A. Kolitsch and M. Remškar, *physica status solidi (b)*, 2009, **246**, 2782-2785.

42. H. Liu, D. Su, R. Zhou, B. Sun, G. Wang and S. Z. Qiao, *Advanced Energy Materials*, 2012, **2**, 970-975.

43. S. Ding, D. Zhang, J. S. Chen and X. W. Lou, *Nanoscale*, 2012, **4**, 95-98.

44. S. Liang, J. Zhou, J. Liu, A. Pan, Y. Tang, T. Chen and G. Fang, *CrystEngComm*, 2013, **15**, 4998-5002.

45. X. Chen, X. Wang, Z. Wang, W. Yu and Y. Qian, *Materials Chemistry and Physics*, 2004, **87**, 327-331.

46. H. Farag, A.-N. A. El-Hendawy, K. Sakanishi, M. Kishida and I. Mochida, *Applied Catalysis B: Environmental*, 2009, **91**, 189-197.

47. P. A. Lieberzeit, A. Afzal, A. Rehman and F. L. Dickert, *Sensors and Actuators B: Chemical*, 2007, **127**, 132-136.

48. R. Farrell, T. Fitzgerald, D. Borah, J. Holmes and M. Morris, *International Journal of Molecular Sciences*, 2009, **10**, 3671.

49. R. A. Farrell, N. Petkov, M. T. Shaw, V. Djara, J. D. Holmes and M. A. Morris, *Macromolecules*, 2010, **43**, 8651-8655.

50. M. Park, C. Harrison, P. M. Chaikin, R. A. Register and D. H. Adamson, *Science*, 1997, **276**, 1401-1404.

51. Q. Fang, X. Li, A. P. Tuan, J. Perumal and D.-P. Kim, *Journal of Materials Chemistry*, 2011, **21**, 4657-4662.

52. T. Ghoshal, R. Senthamaraikannan, M. T. Shaw, J. D. Holmes and M. A. Morris, *Nanoscale*, 2012, **4**, 7743-7750.

53. S. Krishnamoorthy, K. K. Manipaddy and F. L. Yap, *Advanced Functional Materials*, 2011, **21**, 1102-1112.

54. K.-m. Lim, S. Gupta, C. Ropp and E. Waks, *Microelectron. Eng.*, 2011, **88**, 994-998.

55. I. W. Rangelow, *Vacuum*, 2001, **62**, 279-291.

56. Y.-H. Lee, X.-Q. Zhang, W. Zhang, M.-T. Chang, C.-T. Lin, K.-D. Chang, Y.-C. Yu, J. T.-W. Wang, C.-S. Chang, L.-J. Li and T.-W. Lin, *Advanced Materials*, 2012, **24**, 2320-2325.

57. A. Chaudhari, T. Ghoshal, M. T. Shaw, C. Cummins, D. Borah, J. D. Holmes and M. A. Morris, Formation of sub-7 nm feature size PS-b-P4VP block copolymer structures by solvent vapour process, 2014.

58. A. Chaudhari, T. Ghoshal, M. T. Shaw, C. Cummins, D. Borah, J. D. Holmes and M. A. Morris, *Applied Materials & Interfaces*, 2015.

59. C. Cummins, D. Borah, S. Rasappa, A. Chaudhari, T. Ghoshal, B. M. D. O'Driscoll, P. Carolan, N. Petkov, J. D. Holmes and M. A. Morris, *Journal of Materials Chemistry C*, 2013, **1**, 7941-7951.

60. T. Ghoshal, R. Senthamaraikannan, M. T. Shaw, J. D. Holmes and M. A. Morris, *Advanced Materials*, 2014, **26**, 1207-1216.

61. D. C. Bradley, R. K. Multani and W. Wardlaw, *Journal of the Chemical Society (Resumed)*, 1958, 4647-4651.

62. T. H. Fleisch and G. J. Mains, *The Journal of Chemical Physics*, 1982, **76**, 780-786.

63. M. T. Greiner, L. Chai, M. G. Helander, W.-M. Tang and Z.-H. Lu, *Advanced Functional Materials*, 2012, **22**, 4557-4568.

64. M. T. Greiner, M. G. Helander, W.-M. Tang, Z.-B. Wang, J. Qiu and Z.-H. Lu, *Nat Mater*, 2012, **11**, 76-81.

65. W. Gruenert, A. Y. Stakheev, R. Feldhaus, K. Anders, E. S. Shpiro and K. M. Minachev, *The Journal of Physical Chemistry*, 1991, **95**, 1323-1328.

66. A. Katrib, A. Benadda, J. W. Sobczak and G. Maire, *Applied Catalysis A: General*, 2003, **242**, 31-40.

67. A. Soultati, A. M. Douvas, D. G. Georgiadou, L. C. Palilis, T. Bein, J. M. Feckl, S. Gardelis, M. Fakis, S. Kennou, P. Falaras, T. Stergiopoulos, N. A. Stathopoulos, D. Davazoglou, P. Argitis and M. Vasilopoulou, *Advanced Energy Materials*, 2014, **4**, n/a-n/a.

68. M. Vasilopoulou, A. M. Douvas, D. G. Georgiadou, L. C. Palilis, S. Kennou, L. Sygellou, A. Soultati, I. Kostis, G. Papadimitropoulos, D. Davazoglou and P. Argitis, *Journal of the American Chemical Society*, 2012, **134**, 16178-16187.

69. J. F. Moulder and J. Chastain, *Handbook of x-ray photoelectron spectroscopy : a reference book of standard spectra for identification and interpretation of XPS data*, Perkin-Elmer Corporation, Eden Prairie, Minnesota, 1992.

70. M. A. Albiter, R. Huirache-Acuña, F. Paraguay-Delgado, J. L. Rico and G. Alonso-Nuñez, *Nanotechnology*, 2006, **17**, 3473.

71. E. G. da Silveira Firmiano, A. C. Rabelo, C. J. Dalmaschio, A. N. Pinheiro, E. C. Pereira, W. H. Schreiner and E. R. Leite, *Advanced Energy Materials*, 2014, **4**, n/a-n/a.

72. M. A. Baker, R. Gilmore, C. Lenardi and W. Gissler, *Applied Surface Science*, 1999, **150**, 255-262.

73. M. S. Daqiang Gao, Jinyun Li, Jing Zhang, Zhipeng Zhang, Zhaolong Yang, Desheng Xue, *Nanoscale Research Letters* 2013, **8**.

74. H. Li, Q. Zhang, C. C. R. Yap, B. K. Tay, T. H. T. Edwin, A. Olivier and D. Baillargeat, *Advanced Functional Materials*, 2012, **22**, 1385-1390.

75. M. Geske, O. Korup and R. Horn, *Catalysis Science & Technology*, 2013, **3**, 169-175.

76. C. Lee, H. Yan, L. E. Brus, T. F. Heinz, J. Hone and S. Ryu, *ACS Nano*, 2010, **4**, 2695-2700.

77. H. Tributsch and J. C. Bennett, *Journal of Electroanalytical Chemistry and Interfacial Electrochemistry*, 1977, **81**, 97-111.

78. T. J. Wieting and J. L. Verble, *Physical Review B*, 1971, **3**, 4286-4292.

79. L. A. Cosgrove and P. E. Snyder, *Journal of the American Chemical Society*, 1953, **75**, 1227-1228.